Interreg North-West Europe RAWFILL

Co-funded by the Walloon region

I1.3.4 Correlation analysis report

Date: January 2020

SUBJECT:	I1.3.4 Correlation analysis report		
☒ report	☐ information	☐ consideration	☐ decision
To: …		From: ULiège & BGS	

I1.3.4 Correlation analysis report

In this report, we present a correlation analysis between the most relevant geophysical and sampling data obtained in the landfill of Meerhout. The sampling survey was done in two stages: first, 9 boreholes distributed in all the landfill (Figure 1a) and secondly, a trench in the lower eastern zone (Figure 1b). Between these two phases, an additional geophysical survey focused in the lower zone of the site was conducted.

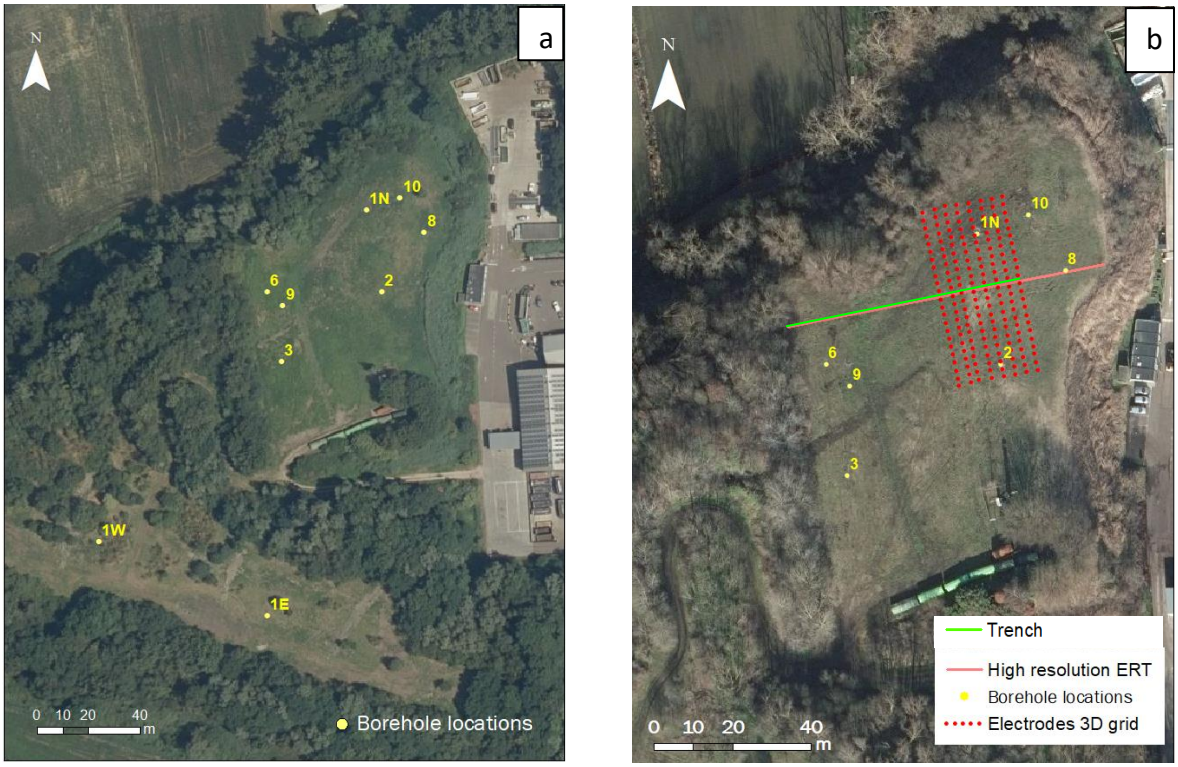

Figure 1. First (a) and second (b) stage of the sampling survey. The boreholes are shown in yellow and the trench in green. The pink line along the trench is the location of a high-resolution ERT/IP profile and the red grid is the 3D ERT survey, both conducted after the first sampling.

First sampling survey

The nine boreholes drilled during the first phase of the sampling (November 2018) are shown in Figure 1a. To study correlation with the sampling data, we mainly use the ERT and IP data acquired during the first geophysical survey January 2018 (see Figure 2 and Deliverable I1.2.2). Selected data

encompass only the lower zone of the landfill. One or two boreholes are available for correlation analysis per ERT/IP profile.

Figure 2. First geophysical survey: in green is shown the location of the ERT/IP profiles, in pink the refraction and MASW profiles and the green dots are the location of the H/V stations.

Based on the sampling results presented in Deliverable I1.3.3, one may mainly distinguish four layers with variable thicknesses within the selected zone. The 1st layer (the shallowest) was predominantly composed of sand, humus, silt, roots and inert waste. The 2nd layer was mainly composed of sand, humus, silt and inert waste, the 3rd layer is the main municipal solid waste (MSW) body including organic wastes, plastics, textile, metals, leather, rubber, parget wastes, glass mixed with sand. The deepest layer is the natural soil composed of moderately coarse sand with moderate clay content (Van Diest formation). The thickness of the MSW body in the lower zone ranges between 10.5 m and 12.8 m whereas in the upper zone it rather ranges between 22.2 m and 23 m (see boreholes 1W and 1E). As the 1st and 2nd layers are very similar in composition and both constitute the cover layer, we choose to merge them in our interpretation. Then, we overlapped the limits of the three layers observed in each borehole (i.e. cover layer, waste body and natural soil) in the ERT/IP models.

As an example, Figure 3 shows the profile P5 (see location in Figure 2) plotted together with the boreholes 2 and 9. A shallow layer of large resistivity values and very low chargeability can be observed, whose thickness correspond to the thickness of the cover layer. The high chargeability layer observed just below can be attributed to the MSW body. Within the MSW body, more resistivity anomalies are

observed which complicates the interpretation. In addition, due to limited depth of investigation it was not possible to map the lower limit of the waste body neither the natural soil.

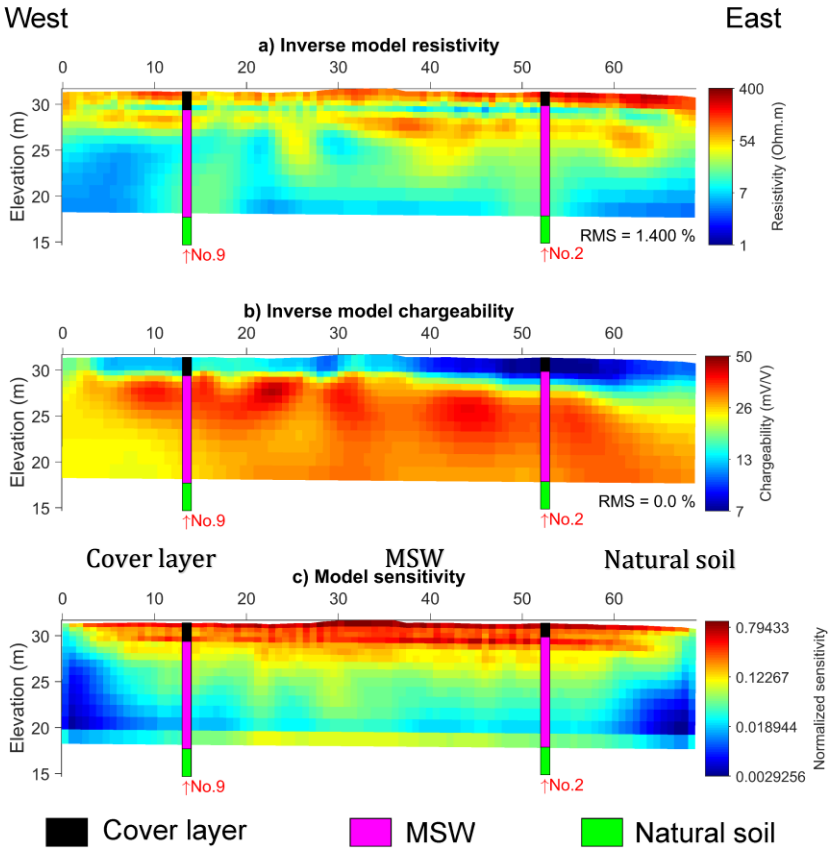

Figure 3. a) Resistivity model, b) chargeability model and c) sensitivity of P5 together with the boreholes 9 and 2. Low chargeability observed corresponds to the cover layer whereas the high chargeability can be attributed to the waste body.

With the 3D ERT model presented in Figure 4, we can also observe the shallow layer of high resistivity values related to the cover layer and the decrease of resistivity with depth due to the MSW body (see grid location in Figure 1b).

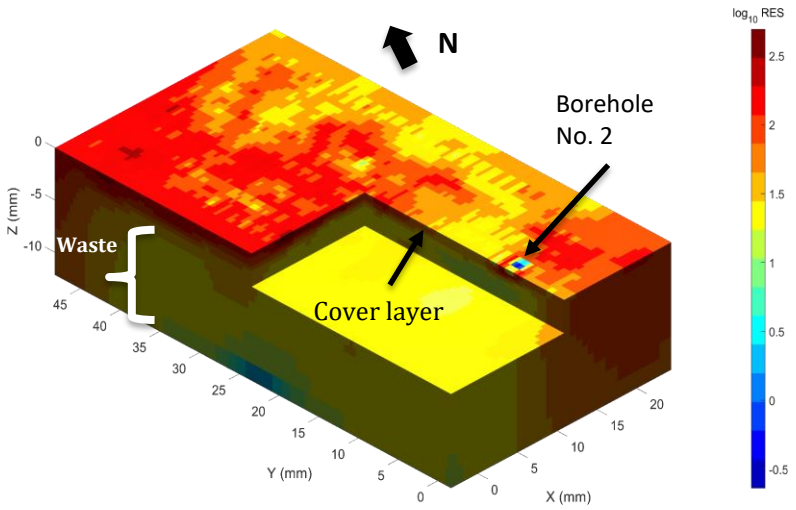

Figure 4. 3D resistivity model in the lower zone of the landfill, see location of the electrodes grid in Figure 1b.

During the drilling, water table was detected at 7.5 m depth in all the boreholes of the lower zone. We reported the water table depth on the resistivity models to see if there were some correlations between the observed anomalies within the waste body and the water table. For example, in profile P1 where boreholes 6 and 3 were drilled, the reported water table corresponds to the decrease in resistivity values observed (see Figure 5). Another example is the resistivity of profile P5 plotted with the water table from boreholes 9 and 2 (see Figure 6). The water table in this case might be discontinuous. Note that as the ERT profiles were not collected at the same time as the drillings, water table might have fluctuated between the two periods. Furthermore, a potential shallower water table

was not caught during the drillings This may explain why there are more than one low-resistivity layers possibly related to the water table, at higher levels than observed in the boreholes.

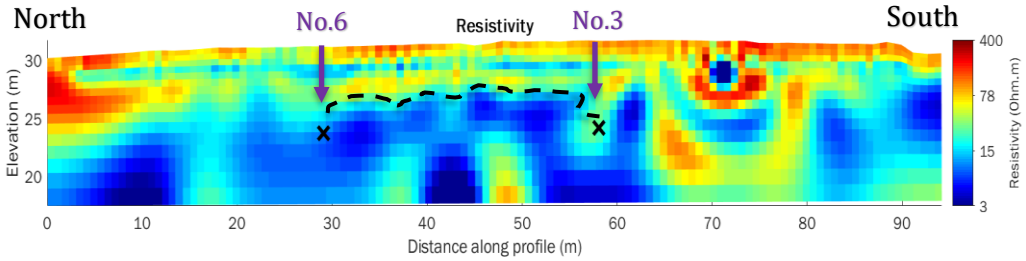

Figure 5. Resistivity model of profile P1. Purple arrows indicate the locations of boreholes 6 and 3, the crosses are the depths of the water table reported in each borehole. The dashed line represents the interpolation of the water table level along the lowest resistivity values.

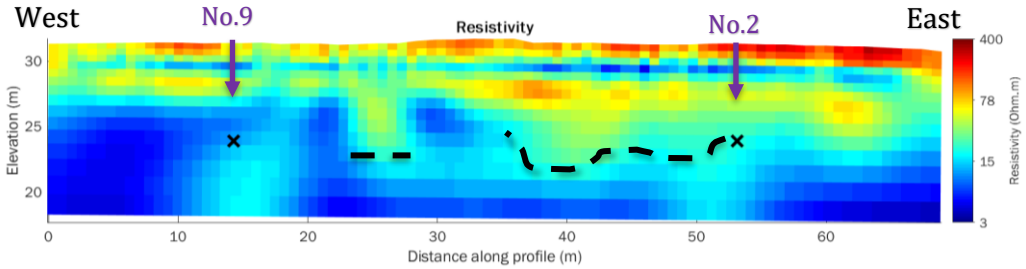

Figure 6. Resistivity model of profile P5. Purple arrows indicate the locations of boreholes 9 and 2, the crosses are the depths of the water table reported in each borehole. The dashed line represents the interpolation of the water table level along the lowest resistivity values.

The more detailed laboratory analyses included a description of all the drill cores with a sampling interval of 2 m. Parameters measured include notably density and moisture content. We use the resistivity sections to check correlations with the moisture content (%) and density (kg/m^3). For example, Figure 7 shows the resistivity section of profile P3, the location of the boreholes 1N and 2 (in solid grey line) and the plots of moisture content *vs* depth at each borehole (black asterisks). The reference value of moisture content was the median for each borehole: 32.65 % for borehole 1N and 22.3% for borehole 2. The overlapped plots of moisture content *vs* depth are centred at the position of each borehole that in turn represent the reference value of moisture content. We notice that borehole 1N, in general, presents larger moisture content values compared to borehole 2. Also, for

both boreholes we can see that the increment in moisture content is related to the decrease of resistivity values and vice versa.

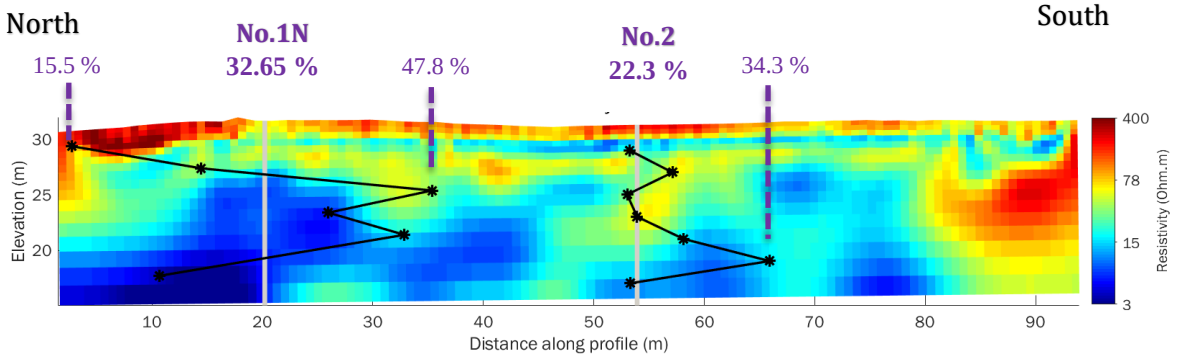

Figure 7. Resistivity section of profile P3 together with the location of boreholes 1N and 2 (grey line). In black, the plots of the moisture content vs depth are shown. 32.65 % and 22.3% are de moisture content mean values for boreholes 1N and 2 respectively. Other values of moisture content are also shown at different depths.

Figure 8 shows the resistivity section of profile P3 using the plots of density *vs* depth. We followed the same procedure than before and computed the two reference values of density: 1446 kg/m^3 and 1914 kg/m^3 for boreholes 1N and 2 respectively. Notice that in this case, the density is larger in borehole 2 than in borehole 1N. Although the changes in the electrical resistivity are more associated with moisture content than with the density (the resistivity decreases with the increase of water content), both moisture content and density can be linked. In general, we notice that the decrease in density is related to the water content. The decrease of density may also be explained by biodegradation processes or different waste composition, but in order to validate this hypothesis further analysis would be required.

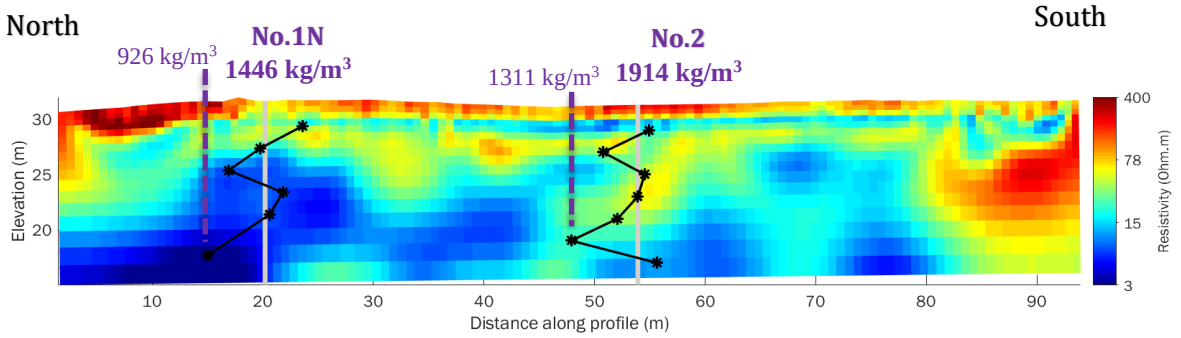

Figure 8. Resistivity section of profile P3 together with the location of boreholes 1N and 2 (grey line). In black, the plots of the density vs depth are shown. 1446 kg/m^3 and 1914 kg/m^3 are de moisture content reference values for boreholes 1N and 2 respectively. Other values of density are also shown at different depths.

In addition to moisture and density, a quantitative analysis of the different waste compounds was also reported every 2 m along the drill cores. The waste categories analysed are: plastic, metal, stones, paper, glass, rubber, polystyrene foam and a category including all "remaining" materials such as soil, sand, wood, etc. Reported values for each category are expressed in percentage of total weight. For most of the boreholes in the lower zone of the landfill, the most represented category is the "remaining" one with 70 % to 98.8% of the total sample mass. Paper, glass, rubber and polystyrene foam are very scarce whereas the plastics, metal and stone contents are large only at a few punctual

depths. In order to study possible correlations between geophysical properties and sampling data, we extracted the resistivity and chargeability values from the models obtained after the first geophysical survey at the specific location of the samples. Then we display the selected parameters in function of the corresponding metal and plastic contents which are expected to impact the most the electrical properties (see Figure 9).

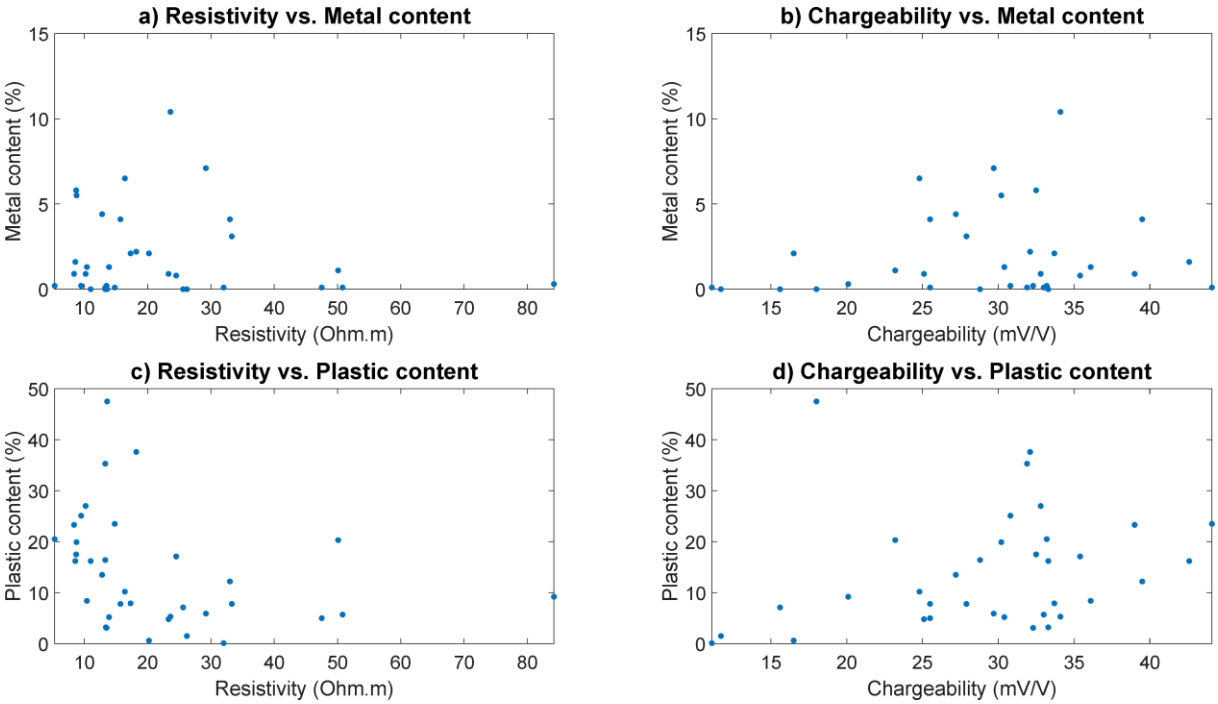

Figure 9. Electrical resistivity and chargeability in function of the plastic and metal contents.

As illustrated in Figure 9, the correlation between electrical properties and metal/plastic content is not straightforward. In order to quantify it, we computed the Pearson correlation coefficients for each combination of parameters (see Table 1).

Table 1: Correlations coefficients between geophysical and sampling data

	Chargeability (mV/V)	Resistivity (Ohm.m)
Metal content (%)	0.14	-0.09
Plastic content (%)	0.25	-0.31

The poor correlation observed between both types of data may be explained by the heterogeneity of MSW waste found in the landfill. In such a context, large variations of waste composition may occur on a very small area. Boreholes provide high resolution data, but at punctual location. The information is therefore not necessarily representative of the whole landfill composition. In contrast, ERT and IP methods offer a higher spatial coverage but with less resolution. All these aspects complicate the correlation analysis between the borehole and the geophysical data. Therefore, most of the anomalies

in the resistivity and chargeability models could not directly be attributed to the content variability of only one waste type (e.g. plastic, metal).

Second sampling survey

Qualitative description of the correlation between ERT/IP models and sampling results

The location of the initially planned trench is displayed in Figure 1b. Due to practical constraints, it was reduced to 7 trial pits with lengths between 3 to 5 m, widths ranging from 2 to 3.5 m and depths of around 3 m. For more details on the sampling and characterization results see deliverable I1.3.3.

During the excavation of the trial pits, 4 layers were identified on the top of the MSW body (layer 5) as shown in Figure 10. As the 7 trial pits (T1-T7) were performed along most of the high-resolution ERT/IP profile (Figure 1b), we firstly overlapped the inverted models of resistivity and chargeability with the boundaries of the observed layers in each trial pit, see Figures 11 and 12. We also represent the bottom limit of the MSW or layer 5 considering the waste thickness reported in the borehole 8 and assuming a flat surface of the natural soil.

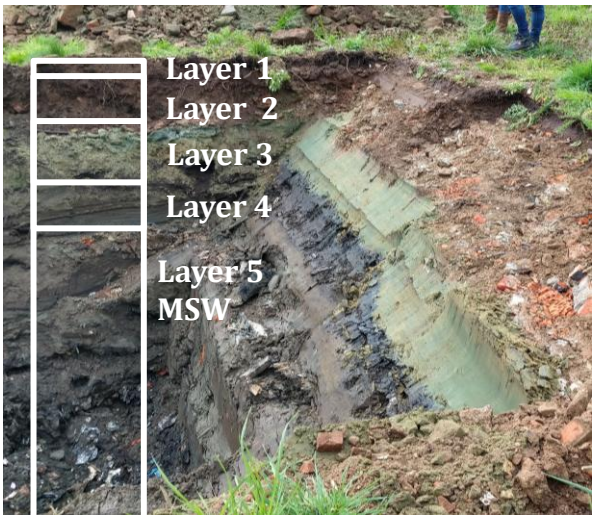

Figure 10. Layering observed in one of the trial pits. Here, 5 different layers can be observed. They are mostly composed of brown dirt, sand, inert waste, some metals and plastics. In the deepest part, the household waste body can be distinguished.

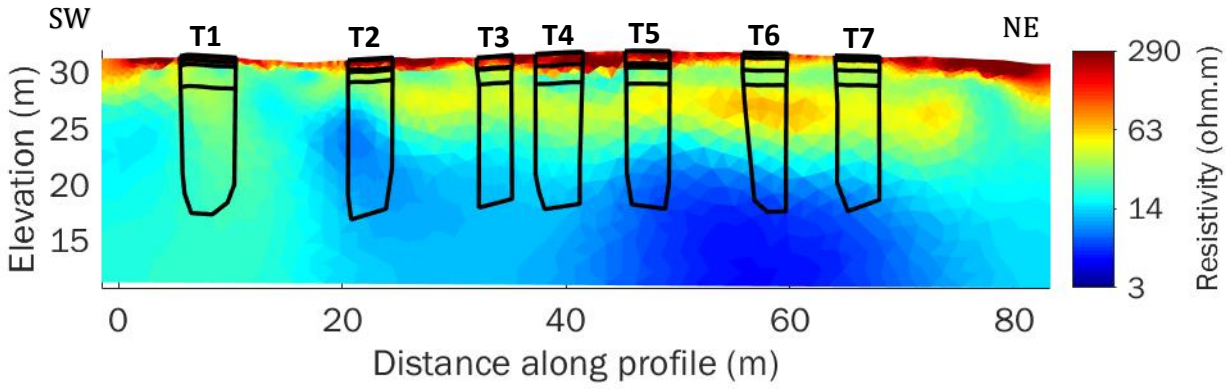

Figure 11. Inverse resistivity model with the contour of the 7 trial pits (T1-T7) and the division of 4 to 5 layers observed during the excavations.

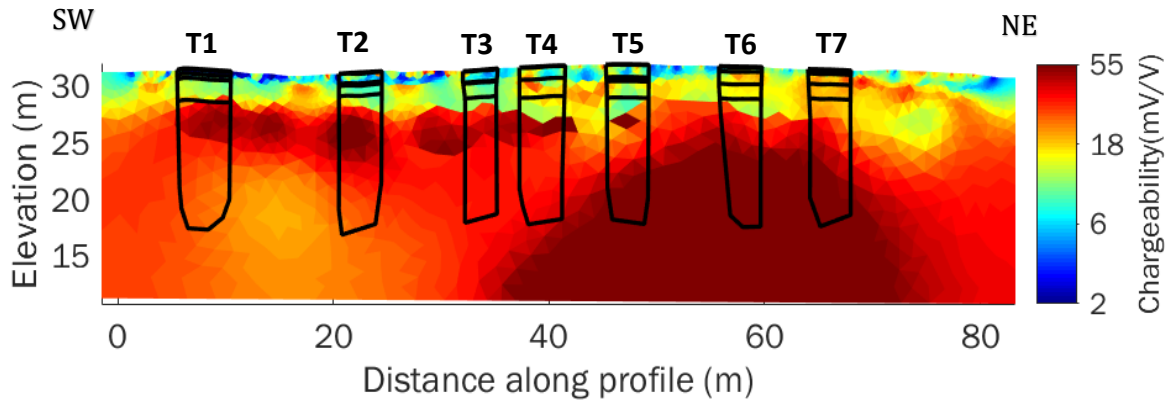

Figure 12. Inverse chargeability model with the contour of the 7 trial pits (T1-T7) and the division of 4 to 5 layers observed during the excavations.

As illustrated in Figure 11, the resistivity model presents a shallow thin layer of higher values that becomes thinner (nearly inexistent) towards the trial pits 6 and 7. This is in agreement with the variable thicknesses and the buried materials of the two first layers reported in T1-T5 and T6-T7. The two first layers of T1-T5 correspond to sand, traces of asbestos, bricks, concrete and debris while T6-T7 is composed of sand and few traces of debris. Thus, we can reasonably state that the highest resistivity values largely correspond to the presence of mixed sand and inert waste. On the other hand, concerning layers 3 and 4, resistivity variations are more difficult to relate to materials composition.

The chargeability model shown in Figure 12 presents heterogeneities in the shallowest part and larger chargeability values starting at a depth of around 4 m. This increment in chargeability roughly coincides (for most of the trial pits) with the top of the MSW body.

In addition, it is important to note that both ERT and IP models exhibit a loss of sensitivity towards the bottom and edges of the model (see Figure 13).

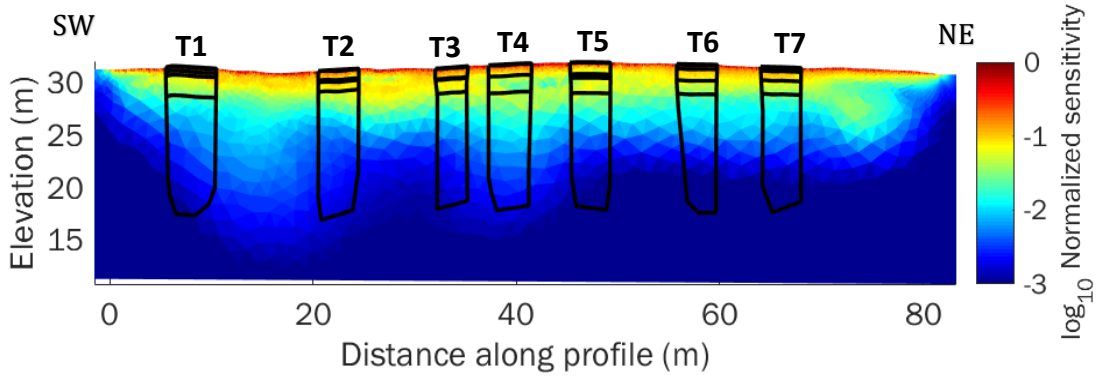

Figure 13. Normalized sensitivity model. The larger the sensitivity value, the more reliable is the resistivity/chargeability model.

Quantitative relationship between ERT/IP models and trial pits

To quantitatively correlate the geophysical models with the information provided by the trial pits we followed a probabilistic approach in order to derive probability maps to find a given material or combinations of different materials (Hermans et al., 2015). Here we present an application of this approach used on the normalized chargeability.

We notice that both ERT and IP models have some features that can be associated with the observed layering in the trial pits, therefore we use the normalized chargeability to develop the probabilistic approach. Normalized chargeability (chargeability divided by resistivity) has been used for instance to quantify the magnitude of surface polarization being closely related to lithology in non-metallic soils (Slater and Lesmes, 2002). The normalized chargeability of the high-resolution profile is illustrated in Figure 14. This model displays characteristics of both the resistivity and chargeability models (Figures 11 and 12): it presents a shallow layer of low normalized chargeability (cover layer) and an increase of these values with depth that can be related with the MSW body. However, the large values of normalized chargeability are strongly influenced by the deepest interface of very low resistivity (Figure 11) that might be related with a layer of higher water content.

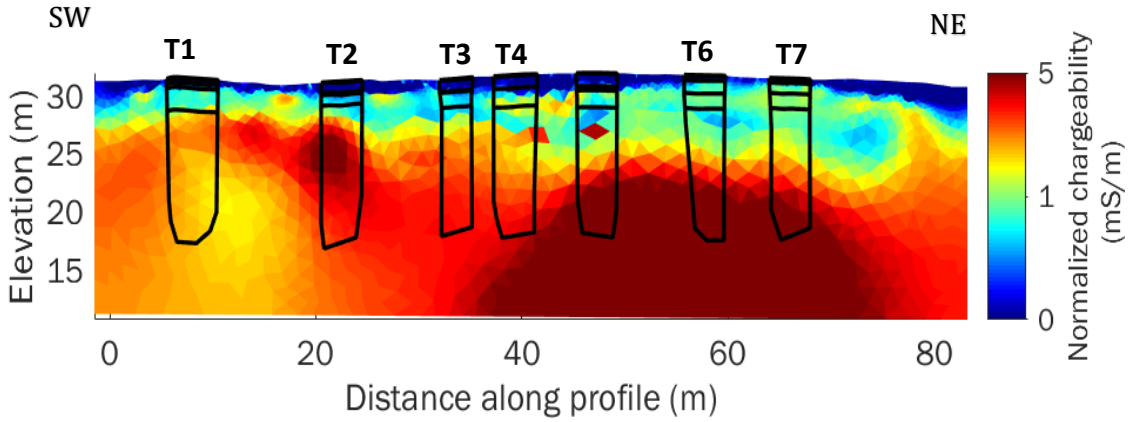

Figure 14. Inverse normalized chargeability model with the contour of the 7 trial pit (T1-T7) and the division of 4-5 layers observed during the excavations.

We followed the probabilistic approach proposed by Hermans and Irving (2017). First, we compare the normalized chargeability model with the co-located data from the trial pits through the computation of histograms for each of the 5 observed layers (see Figure 15). With the histograms we notice that it is not possible to differentiate between layers 1 and 2 as the shallowest layer -mainly composed of grass and brown dirt- is too thin (~5cm) to be resolved. We can also see that layers 3 and 4 are mostly overlapped but layer 5, corresponding to MSW, presents the largest values of normalized chargeability and can be distinguished from the rest.

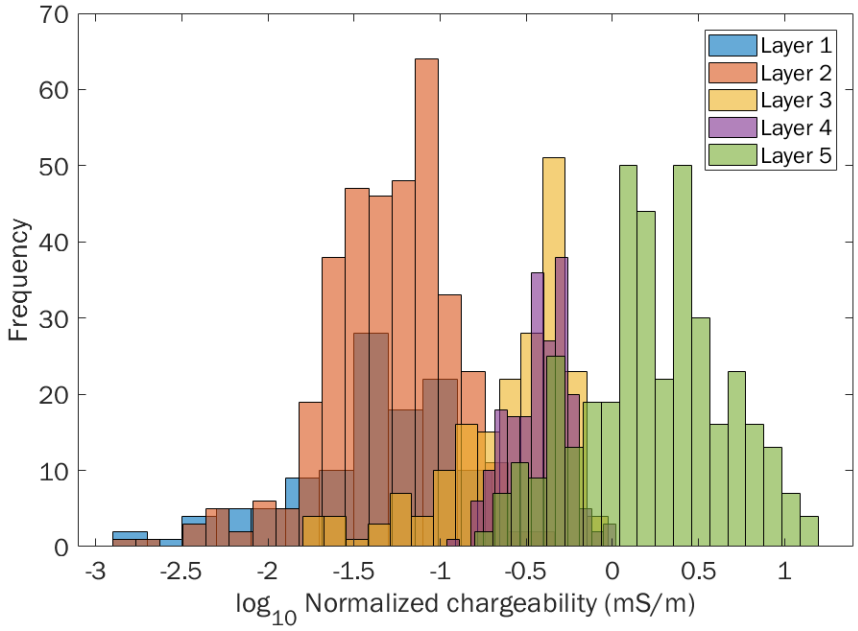

Figure 15. Histograms of the normalized chargeability model for each of the 5 layers identified in the 7 trial pits.

Afterwards, we computed 3 conditional probabilities given the normalized chargeability, after grouping layers 1-2, layers 3-4 and layer 5 (see Figure 16, solid lines). We notice that the normalized chargeability values smaller than 10^{-1} have a probability close to 1 of being part of the shallowest cover layer of the landfill. On the other hand, normalized chargeabilities larger than 0 are most probably part of MSW or layer 5.

In addition, we can consider the effect of the sensitivity (logarithm of normalized sensitivity in this case, see Figure 13) on the conditional probabilities. We first divided the sensitivity domain in several step ranges and then we used Bayes' rule to compute sensitivity-dependent distributions in each sensitivity step (Hermans and Irving, 2017). For example, Figure 16 shows in dashed lines, the conditional probabilities of the different layers given the normalized chargeability and a sensitivity range between -1.69 and -0.84. The sensitivity correction using this step had almost no effect on the conditional probability of layers 1 and 2, meanwhile, we see a decrement in the conditional probability of layers 3 and 4. In general, the conditional probabilities after applying the sensitivity correction become broader meaning that it is more difficult to resolve normalized chargeabilities between different layers.

On the other hand, we can also represent the former distributions as probability 2D maps considering the full normalized chargeability model space. Then, depending on the structural characteristic we want to examine, we may estimate the probability from 0 to 1 of having MSW or the materials from the shallowest cover layer at specific locations. For example, we can take the conditional probability of the MSW, given the normalized chargeability and sensitivity, and map the entire model domain to get the probability map displayed in Figure 17. In this map, the cover layer (or lack of MSW) is reflected with probabilities close to 0 meanwhile the largest probability values reflect the waste presence. Notice that we could not delineate the bottom limit of the waste by using ERT/IP. However, we applied a transparency filter in the probability map of Figure 17 for sensitivity values smaller than -2.7.

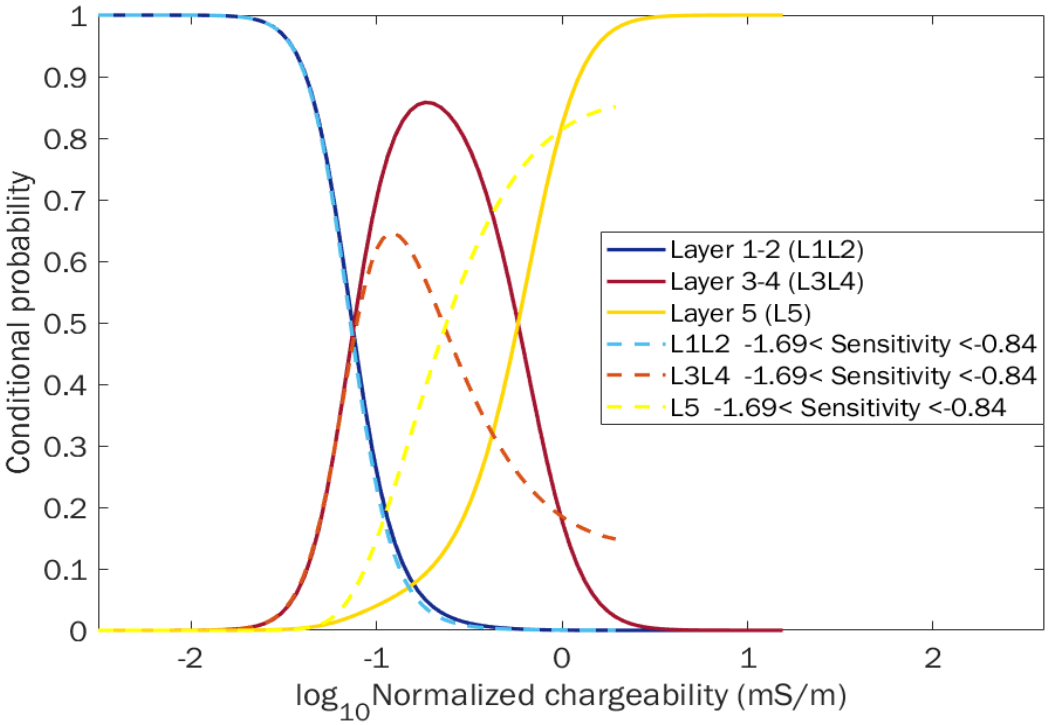

Figure 16. Conditional probability of layers 1-2, layers 3-4 and layer 5 given the normalized chargeability (solid lines). Dashed lines show the conditional probabilities of the same sets of layers given the normalized chargeability and a sensitivity range between -1.69 and -0.84.

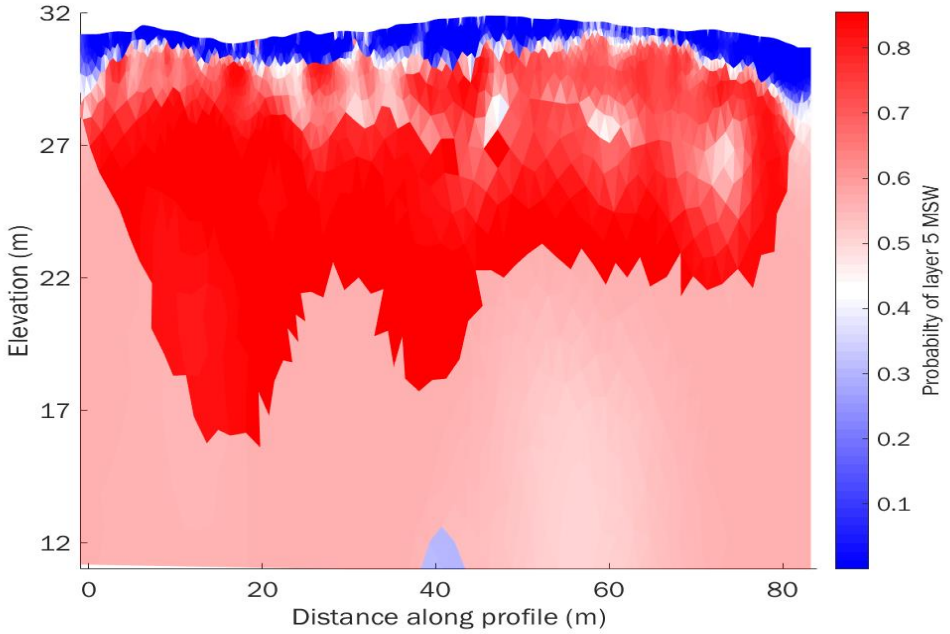

Figure 17. Probability map of the MSW or layer 5, applying a transparency for values of sensitivity < -2.7.

Conclusions

First, the resistivity and chargeability models could be correlated with the general structure of the landfill trough a probabilistic methodology. The larger resistivity values in the shallow zones can be linked with the cover layer and the largest chargeability values are associated with the main MSW body. However, due to the acquisition settings of the profiles (i.e. electrode spacing, array) and their sensitivity, it was not possible to map the interface between the waste and the natural soil underneath.

With the profiles of the first geophysical survey (low resolution), we believe that the resistivity anomalies within the waste can largely be linked to the moisture content and/or the presence of the water table. However, it is not possible to link the resistivity and chargeability variations with the changes in only one type of waste content (plastic, metals, paper, etc.). The shallowest zone of the resistivity models ‐presenting low values- might be related to the low water content near the surface.

The high-resolution profile images well the heterogeneities of the subsurface especially in the chargeability model. We believe that higher resolution ERT/IP profiles (depending on the targeted depth) could be useful to explore MSW landfills together with ground truth data from boreholes (and lab analysis of samples taken at shorter intervals than every 2m). Finally, although the general structure of the landfill can be imaged with geoelectrical methods, our data do not allow to distinguish the geophysical signature of the different materials composing the MSW landfill individually.

Reference

Hermans, T., Nguyen, F., & Caers, J. (2015). Uncertainty in training image ‐ based inversion of hydraulic head data constrained to ERT data: Workflow and case study. Water Resources Research, 51(7), 5332-5352.
Hermans, T. and Irving, J. (2017). Facies discrimination with ERT using a probabilistic methodology: effect of sensitivity and regularization. Near Surface Geophysics, 15, 13-25.
Slater, L., & Lesmes, D. P. (2002). Electrical ‐ hydraulic relationships observed for unconsolidated sediments. Water Resources Research, 38(10), 31-31-31-13.

Contact

Feel free to contact us.

Local contact details:

BELGIUM	ATRASOL	renaud.derijdt@gmail.com
	i-Cleantech Vlaanderen	annick.vastiau@i-cleantechvlaanderen.be
	OVAM	ewille@ovam.be
	SPAQuE	c.neculau@spaque.be
	Université de Liège	f.nguyen@ulg.ac.be
FRANCE	SAS Les Champs Jouault	champsjouault@gmail.com
GERMANY	BAV	wolf@bavmail.de
THE UK	UKRI	jecha@bgs.ac.uk

Coordination office:

BELGIUM	SPAQuE Boulevard d' Avroy 38 4000 Liège	c.neculau@spaque.be